Biogeosciences Discuss., 8, 5563–5585, 2011
www.biogeosciences-discuss.net/8/5563/2011/
doi:10.5194/bgd-8-5563-2011

Biogeosciences Discussions

Confocal Raman microscopy as a tool to describe different mineral and organic phases at high spatial resolution within marine biogenic carbonates: case study on *Nerita undata* (Gastropoda, Neritopsina)

G. Nehrke[1] **and J. Nouet**[2]

[1]Alfred Wegener Institute for Polar and Marine Research, Am Handelshafen 12, 27570 Bremerhaven, Germany
[2]University Paris Sud, IDES UMR8148, Bâtiment 504, Campus Universitaire, 91405 Orsay Cedex, France

Received: 20 May 2011 – Accepted: 28 May 2011 – Published: 9 June 2011

Correspondence to: G. Nehrke (gernot.nehrke@awi.de)

Published by Copernicus Publications on behalf of the European Geosciences Union.

Abstract

Marine biogenic carbonates formed by invertebrates (e.g. corals and mollusk shells) represent complex composites of one or more mineral phases and organic molecules. This complexity ranges from the macroscopic structures observed with the naked eye down to sub micrometric structures only revealed by micro analytical techniques. Understanding to what extent and how organisms can control the formation of these structures requires that the mineral and organic phases can be identified and their spatial distribution related. Here we demonstrate the capability of confocal Raman microscopy applied to cross sections of a shell of *Nerita undata* to describe the distribution of calcite and aragonite including their crystallographic orientation with high lateral resolution (~ 300 nm). Moreover, spatial distribution of functional groups of organic compounds can be simultaneously acquired, allowing to specifically relate them to the observed microstructures. The data presented in this case study highlights the possible new contributions of this method to the description of modalities of *Nerita undata* shell formation, and what could be expected of its application to other marine biogenic carbonates. Localization of areas of interest would also allow further investigations using more localized methods, such as TEM that would provide complementary information on the relation between organic molecules and crystallographic lattice.

1 Introduction

Carbonates formed by marine calcifying organisms like e.g. corals and mollusks, received much attention in the field of biogeosciences during the last decades. On the one hand they represent important proxy archives e.g. oxygen isotopic composition can be used for temperature reconstruction (McCrea, 1950; Urey et al., 1951) and on the other hand they are affected by the increasing acidification of the ocean (a process commonly termed ocean acidification, OA), due to increasing atmospheric CO_2 concentrations (Royal Society, 2005). To evaluate the possible consequences of OA

BGD
8, 5563–5585, 2011

on the marine calcifying fauna it is essential to understand the interplay of cell physiological processes and crystal nucleation leading to the formation of their calcareous structures.

It has long been shown that biogenic carbonates constitute complex composites of organic and inorganic components (Crenshaw, 1972; Gregoire, 1960). As demonstrated by previous studies using Scanning Electron Microcopy (SEM), Transmission Electron Microscopy (TEM), and Atomic Force Microscopy (AFM), organic compounds are incorporated within the mineral phase down to the sub-micrometer scale (Mutvei, 1969; Weiner and Traub, 1984). Apart from the fact that organic molecules are intimately associated to the mineral phase within biogenic carbonates, it is not known to what extent these molecules are involved in the control of mineralogy and shape during the biomineralization processes. Thus, the identification of the organic molecules and their spatial distribution within the biogenic carbonate is the basic step for a processed based understanding of biomineralization. For the interpretation of culture experiments using e.g. corals or mollusks performed under artificially altered CO_2 levels, like often done in OA research, it is mandatory to be able to precisely illustrate small microstructural changes and correlate them to the biochemical composition. However, analytically it is challenging to obtain this information.

The use of various dyes or etchings together with light microscopy, SEM, or TEM can give some information on the spatial distribution of organic structures but without a chemical characterization of the organic components (Cuif et al., 2011). Methods like e.g. synchrotron based X-ray Absorption Near Edge Structure (XANES) or Time Of Flight-Secondary Ion Mass Spectroscopy (TOF-SIMS) can give chemical information about organic compounds with high spatial resolution (Cusack et al., 2008; Dauphin et al., 2008, 2010; Farre et al., 2011; Heim et al., 2009), but are either difficult to access (XANES) or prone to contamination (TOF-SIMS). Extracts of organic compounds from biogenic materials allow a better characterization of their composition, but nothing can be said about their spatial distribution (Dauphin and Denis, 2000; Farre and Dauphin, 2009; Krampitz et al., 1976; Samata et al., 1980).

BGD
8, 5563–5585, 2011

Confocal Raman microscopy (CRM) represents a method with a good spatial resolution (~ 250 nm) and the ability to determine composition and spatial distribution of many inorganic and organic compounds simultaneously, requiring only simple sample preparation. Within a single acquisition identification of the mineral phases and their repartitions can be achieved and constraints can be given on fine crystallographic parameters such as crystallinity or crystal-units orientations. In addition the biochemical composition can be mapped and related to the microstructural observations. In this regard, CRM represent a very integrated and unique device to address the wide range of questions, which are regularly raised in studies on biogenic structures, including OA experiments.

In order to demonstrate the capability of what results can be achieved using CRM on biogenic carbonates, this case study has been carried out on the shell of *Nerita undata* (Gastropoda, Neritopsina). This taxa is indeed representative of the complexity that can usually be found within molluscan shells, as it presents both simple and complex 3-D microstructural architectures with homogeneous/prismatic and crossed-lamellar layers, as well as different mineral phases (calcite and aragonite) and organic compounds.

2 Material and methods

2.1 Specimen *Nerita undata*

A *Nerita undata* (Linnaeus, 1758) (Gastropoda, Neritopsina) shell (Fig. 1a) has been collected at the Tuamotu Islands, French Polynesia. The shell is composed of an outer calcitic and an inner aragonitic layer (Fig. 1b, c). The calcite layer is usually described as composed of highly irregular, very fine and undulating prisms (Bøggild, 1930). The aragonite layer is crossed-lamellar.

Crossed-lamellar is undoubtedly the microstructure most commonly found in both gastropods and bivalves shells (Bøggild, 1930; Taylor et al., 1969), although many

BGD
8, 5563–5585, 2011

studies on biocrystallization mechanisms have been focused on taxa presenting nacreous and/or prismatic layers (Dauphin et al., 2008; Nakahara and Bevelander, 1971; Nudelman et al., 2006; Travis, 1968). It presents a complex three dimensional architecture, composed of interlaced units at several distinct orders of magnitude. Although many species specific variations exist in size, shape, and orientation, the basic pattern of crossed-lamellar structures is identical. The largest structural unit (termed first order lamellae) is usually described as 10–20 µm large lamellae, showing alternating crystallographic orientation every two lamellae (Bøggild, 1930; Kobayashi, 1964). They are themselves composed of 200 nm thick sheet-like arrangements (termed second order lamellae) of individual rods (which are themselves termed third order lamellae: (Taylor et al., 1969; Kobayashi and Akai, 1994). The third order rods usually dip in opposite directions between two consecutive first order lamellae, with a constant angle that is taxa-related (Taylor et al., 1969; Wilmot et al., 1992). *Nerita undata* inner layer displays a simple, continuous and mostly regular crossed-lamellar microstructure; first order lamellae are very regular and straight lined, perpendicularly to the inner border of the shell (Bøggild, 1930). A radial section across the shell (Fig. 1c), which will be perpendicular both to growth layers and first order lamellae, is therefore well suited for micro structural investigation. In this orientation the typical alternate crystal orientation of first order lamellae can be nicely illustrated using Polarized Light Microscopy (PLM) and crossed polars on thin sections (~ 10 µm thick): the lamellae presenting the exact same crystallographic orientation are simultaneously extinct and display no birefringence colours (Fig. 1d).

Two radial sections were cut close to the peristome of the shell, on the thick lobe that forms the outer lip (Fig. 1b). A first section was glued on a glass plate, then cut and polished using HERMES water grinding papers (grain size P1200/P2500 to P4000) until a ~ 10 µm thick thin section is obtained (sample used for scans labeled scan1a to scan1c in Table 1). Further thick sections were polished using HERMES water grinding papers (grain size P1200/P2500 to P4000), Buehler diamond polycrystalline suspensions (3 µm and 1 µm) and finally aluminium oxide suspension (~ 0.3 µm). Sample

BGD
8, 5563–5585, 2011

surface was carefully rinsed using demineralized water (sample used for scans labeled scan2a and scan2b in Table 1).

2.2 Confocal Raman microscopy

Raman mapping was done using a WITec alpha 300 R (WITec GmbH, Germany) confocal Raman microscope. Scans with a high spatial resolution are performed using a piezoelectric scanner table having a maximum scan range of 200 × 200 µm and a minimum step size of 4 nm lateral and 0.5 nm vertical. Large area scans are performed using a motorized scan table having a maximum scan range of up to 2.5 × 2.5 cm and minimum step size of 100 nm. Details on the type of scans performed are given in Table 1. Lasers of two different wavelengths (532 nm and 785 nm) are used for the scans performed in this study. At each wavelength a dedicated ultra high throughput spectrometer (UHTS 300, WITec, Germany) was used. The spectrometer for 532 nm excitation wavelengths was used with a grating, 600 mm^{-1}, 500 nm blaze and the spectrometer for 785 nm excitation wavelength with a grating, 600 mm^{-1}, 750 nm blaze. The spectrometer for 785 nm excitation wavelength was equipped with a deep depletion CCD since they show a better performance in the NIR region. Many biogenic materials show strong fluorescence using an excitation wavelength of 532 nm which is often reduced using one of 785 nm. The advantage of an excitation wavelength of 532 nm on the other side is the lager spectral range covered during one measurement, making it possible to measure vibrational modes down to 70 cm^{-1} (typical for lattice vibrations of inorganic compounds) and up to 3600 cm^{-1} (typical for vibrational modes of functional groups like e.g. $=CH_2$, 3000–3200 cm^{-1}) simultaneously. Using an edge filter (used to filter out the elastic scattered photons) which cuts of very close to the excitation wavelength, renders a phase identification of calcium carbonates straight forward using their internal and external vibration modes (Behrends et al., 1995; Bischoff et al., 1985). The identification of organic compounds is done via the vibrational modes of their functional groups and less straight forward, since the vibrations strongly depend on their interaction with their nearest environment. However, in

BGD
8, 5563–5585, 2011

the Results and Discussion section it will be shown which information can be obtained from the Raman spectra.

The spectral analysis and imaging processing was done using the WITecProject software (verion 2.04, WITec GmbH, Germany). The peak positions given are determined using the "Mulipeak Fitting 2" routine of IGOR Pro (version 6.11, WaveMetrics, Inc. USA).

3 Results and discussion

3.1 Spatial distribution of mineral phases and crystallographic orientation

Within the spectral dataset of scan1a performed across the zone of progressive transition between outer and inner shell layer (compare structures shown in Fig. 1c), calcite and aragonite could be identified. Calcite was identified using the two lattice modes (translation mode T_c, 155 cm^{-1} and liberation mode L_c, 282 cm^{-1}) and the two internal modes (in-plane band ν_4, 711 cm^{-1} and symmetric stretch ν_1, 1085 cm^{-1}) (Fig. 2a). Aragonite was identified by the two lattice modes (translation mode T_a, 152 cm^{-1} and liberation mode L_a, 206 cm^{-1}) and the two internal modes (in-plane band ν_4, 705 cm^{-1} and symmetric stretch ν_1, 1085 cm^{-1}) (Fig. 2a). The peak positions are in very good agreement with the published literature values (Behrends et al., 1995) and standard materials (information on the standard material used can be found in Kranz et al., 2010). For aragonite two significant different spectra could be identified within the spectral dataset having identical peak positions but different ratios between the peak belonging to the T_a mode and the peaks belonging to the L_a, ν_4, and ν_1 mode. The latter is caused by different crystallographic orientation of the aragonite crystals (from here on referred to as aragonite_a and aragonite_b). The separate maps of the spatial distribution of calcite (b) aragonite_a (c) and aragonite_b (d) and a composite of all three maps (e) is given in Fig. 2. The analysis of the spectral dataset of the depth scan (scan1b) performed along the transect shown in Fig. 2e identifies the presence

BGD
8, 5563–5585, 2011

of aragonite and calcite as the only two mineral phases (Fig. 2f). The transition between calcite and aragonite phases is found to be sharp and oblique; however, a zone presenting no specific crystallographic orientation, ∼ 10 µm thick, is found at the very beginning of the aragonite layer, before the alternation between aragonite a and b orientations starts.

Those results are in good agreement with the known structure of the shell of *Nerita undata*: a calcite outer layer, very irregularly shaped, as well as a systematic alternate orientation of aragonite lamellae within the inner layer. The sharp change of orientation in aragonite strictly corresponds to observations using PM with crossed polars (Fig. 1d). However, new data can be highlighted: with the lateral resolution of the scan, (∼ 300 nm), the change of mineralogy is almost instantaneous, as it occurs in less than a micron, which emphasize the close control exerted over the mineral phase deposited at each growth step. But the change of micro-structural arrangement is not as immediate: the classical interspersed orientation of first order crossed-lamellae can only be established after several micrometers (a few growth increments) of a seemingly homogeneous aragonite layer with no particular orientation.

3.2 Organic compounds

Raman spectra of inorganic compounds like calcite and aragonite consist of relatively few peaks. These peaks can easily be attributed to the different vibrational modes using the Raman spectra of standard materials. The identification of complex organic molecules like the ones present in biogenic materials is difficult. On the one hand standards of these dedicated compounds are not available on the other hand does the peak position of a functional group also depend on the chemical environment. However, even though not the complete spectrum of an organic substance is available, functional groups can often be identified using the position of single peaks. The information obtained by analyzing the geometrical features of single peaks often can give valuable information as will be shown below. The distribution of aragonite having two different crystallographic orientations as shown in Fig. 2c, d was obtained using the

BGD
8, 5563–5585, 2011

complete spectral information of the aragonite spectra (using the basic analysis routine of the WITec Project software package). The same information can be obtained by only analyzing the peak area of the two lattice peaks of aragonite (translation mode T_a, 152 cm^{-1} and liberation mode L_a, 206 cm^{-1}) as illustrated in Fig. 3a–c. It can even be seen that the map based on the intensity distribution (peak area) of only one peak reveals details in the transition zone (Fig. 3a, b) not seen in the map based on the complete spectral information (Fig. 2c, d). The mineral phase in the upper dark area of Fig. 3d is calcite. The next sub-sections describe the information on organic molecules which can be obtained by analyzing the different spectral datasets measured (Table 1).

3.2.1 Fluorescence

Fluorescence induced by organic molecules often represents a severe problem in Raman microscopy. On the other hand, mapping the distribution of fluorescence can reveal information not obtained by the analysis of pronounced peaks. To do so the intensity within an area containing no pronounced peaks should be chosen (for this sample 2400–2500 cm^{-1}). This was done for the spectral dataset of scan2a before any background subtraction was applied. The areal distribution of the fluorescence obtained in the area of scan2a is shown in Fig. 3d. Although no distinction can be made between organic classes, strong banding within the calcitic layer can be identified, that can also be followed within the aragonitic layer even though more faintly marked: These bands correspond exactly to the growth layering of the shell. Irregularities seen in the upper part of Fig. 3d are most probably artifacts from the polishing process during which aggregates of organic particles where formed. These particles would be expected to have some stickiness making it difficult to remove them from the surface without altering it.

BGD
8, 5563–5585, 2011

3.2.2 Pigments; resonance Raman spectroscopy

After the areas showing enhanced fluorescence have been identified (Fig. 3d) the spectral dataset scan2a was examined in these regions. The Raman spectra (Fig. 3e) in some regions of enhanced fluorescence showed several peaks not related to a calcium carbonate mineral phase (1019, 1134, 1525, 2259, 2645, and 3038 cm^{-1}) which are not related to the spectra of calcite or aragonite, but are characteristic for Resonance Raman (RR) spectra from molecules presenting a central polyenic chain (as in β-carotene). Such molecules have been described to be present in some biogenic carbonates, and are usually identified as pigments close to polyenes or carotenoids (Fritsch and Karampelas, 2008; Hedegaard et al., 2005; Urmos et al., 1991). Intensity of the RR bands of these pigments is enhanced compared to the bands caused by the carbonate matrix. The reason for the latter is the resonant coupling of vibrational and electronic transitions with the laser source, which makes it possible to detect very small traces of pigments (down to 10^{-8} M) present within the sample (Merlin, 1985). Some authors attributed very similar RR bands in biogenic carbonates to carotenoids (Fritsch and Karampelas, 2008; Merlin, 1985; Urmos et al., 1991). However, more specific studies (Fritsch and Karampelas, 2008; Hedegaard et al., 2005; Karampelas, 2008) highlight a slight shift from carotenoids standard RR bands, that can be induced by the length of the polyenic chain, number of functional groups attached, or cis-/trans-conformations. These results highlight the potential complexity of pigment identification within biogenic carbonates, which can present assemblages composed by several polyenic pigments (Karampelas, 2008). Using the relation between the positions of C–C single bond and C=C double bond peaks established by Hedegaard et al. (2005) for some all-trans polyenes with various chain lengths and several carotenoids, we consider that these peaks in *Nerita undata*, shown at 1134 and 1525 cm^{-1}, respectively, are most probably produced by polyenes with chains of ~ 9–10 conjugated double bonds and terminal $-CH_3$ groups. The RR effect depends on the wavelength of the laser source (Fritsch and Karampelas, 2008) and in our sample RR peaks could only

BGD
8, 5563–5585, 2011

be observed using the 532 nm excitation wavelength but not with 785 nm excitation wavelength. Since these six peaks have shown to be present in constant ratios to each other one peak (1525 cm^{-1}) was chosen representative to map their distribution (green area Fig. 3f). Figure 3f shows that polyenes are present in a ~40 µm wide area within the calcitic layer along the interface to the aragonitic layer. Plotting the distribution of the polyenes together with the mineralogical phases allows a very precise description of their areal distribution (Fig. 3f): while still following growth layering, they are highly enriched in the calcitic layer, just before the sharp transition to the aragonitic parts. These results exemplify the possibility to correlate localized mineralogy and the distribution of organic molecules at high areal resolution, giving significant new insights on the modalities of shell formation. The mapping of the growth layering therefore allows a timely resolve visualization of the successive growth increments (Fig. 3d). In this particular case, it is clear that a strong change of quantity/type of polyenes is observed before the actual sharp shift from the calcitic layer to the aragonitic layer.

As can be seen from Fig. 3g, which was prepared from the large area scan2b (including the area in which scan2a was performed), the polyenes are strongly sensitive to the Raman measurement and can easily be bleached out of the sample surface (area f Fig. 3g). The calcitic area in Fig. 3g, reconstructed from the intensity of liberation mode L_c, 282 cm^{-1} reveals very fine, fiber-like arrangements within the outer shell layer. Figure 3g also shows the presence of polyenes (based on the peak at 1525 cm^{-1}) within aragonitic inner layer, mostly following the growth lines orientation (Fig. 3g). These details could not be visualized in the high resolution scan and demonstrate the need of scanning larger areas for a good overview of the structures present. On the other hand, like it will be shown in the next section, some information can only resolved performing a scan with high areal resolution.

3.2.3 –C–H groups

The spectral analysis of scan1c was used to determine the mineralogical domains (Fig. 4b). The latter show the same distribution described for the other scans. However,

BGD
8, 5563–5585, 2011

in addition to the peaks belonging to the calcium carbonate phases additional peaks are observed between 2850–3000 cm^{-1} (Fig. 4a), which correspond to the spectral range for −C−H groups stretching vibrations (Smith et al., 2005). A map of this spectral range reveals the presence of highly enriched zones just after the calcite to aragonite transition, as well as their presence within the inner layer (Fig. 4c). Again, a close comparison with the mineralogical information reveals that the compounds containing −C−H groups would be preferentially located between first order lamellae or within the homogeneous aragonitic zone that follows the calcite-to-aragonite transition.

3.2.4 Full width half maximum

The mapping of the full width half maximum (FWHM) of the symmetric stretch v_1 of carbonate group at 1085 cm^{-1} reveal very sharp lines within the calcitic domains (Fig. 3h) which are also visible in the aragonitic domains, even though less pronounced. Surprisingly these growth lines visible in the aragonitic domains correspond partly to the growth lines visualized by the polyenes (se arrows in Fig. 3g). Although it is not clear at the moment what causes these changes in the FWHM of the peak related to the symmetric stretch v_1 of carbonate group at 1085 cm^{-1}, this feature could also be used to follow the growth layering of the shell.

3.3 Evaluation of experimental parameters

In this section we will summarize how sample preparation and experimental parameters affect the results obtained by CRM when measuring polished cross sections of *Nerita undata*. This information will help to identify important aspects which have to be considered if CRM measurements are performed on biogenic carbonates.

1. RR peaks of polyenes are only observed using an excitation wavelength of 532 nm but not 785 nm.

BGD
8, 5563–5585, 2011

2. Both wavelengths (532 and 785 nm) could be used without inducing strong fluorescence. With dedicated studies using different excitation wavelengths and looking at slight shifts or changes of intensities of polyenic chains bands (as suggested by Fritsch and Karampelas, 2008), it might therefore be possible to further investigate the complexity of multiple pigments assemblages and to determine their areal distribution.

3. Peaks belonging to the polyenes are easily bleached away during the measurements.

4. Mapping the fluorescence distribution across the sample gives important structural information even though an exact identification of the substances causing it is not possible.

5. Calculating the FWHM of the peaks related to the symmetric stretch ν_1 of carbonate group at 1085 cm^{-1} reveals structures related to the growth layering. In some parts of the samples this lines correlate with the position of the polyenes, but do not disappear when the polyenes are bleach away.

6. The areal distribution of $-C-H$ groups could only be determined in one of the both samples. This demonstrates that sample preparation (one being a thin section the other a thick section) may alter the sample. Therefore it will be necessary to test different methods of sample preparation to determine which steps during the preparation of a polished surface alter the measured Raman spectra.

4 Conclusions

Our results highlight the potential of CRM for the identification of micro-structural patterns within biogenic carbonates, including mineral phase detection and crystallographic orientation contrasts, as well as distribution of organic content and possible leads toward their identification.

BGD
8, 5563–5585, 2011

When applied to the example of *Nerita undata* shell, a detailed description of modalities of shell deposition can be drawn, involving the variation of secretory activity of different organic molecules from distinct mantle areas through time, as well as a very close control over mineral phase selection and orientation.

Further investigations, dedicated to a better characterization of organic molecules and functional groups (with the use of simple proteins, lipids and sugars standards, or even separated shell extracts) are of course mandatory, as well as investigations on their possible interactions with mineral phases: this way only, complex features, like the variation of FWMH of CO_3^{2-} symmetrical stretch band accordingly to growth layering directions, could be fully explained.

Organic molecules are found to be very sensitive to laser exposition, and can be easily altered or bleached away, urging the need to develop more cautious preparation and measurement protocols (e.g. low laser energy).

This taken into account, using CRM on other biogenic carbonates, such as coral skeletons, foraminifera tests, fish otoliths etc. can be considered to give new insight into their structural composition, enabling a systematic comparison between taxa/phyla, as well as evaluations of the impacts of cultures under artificially altered conditions (OA).

Acknowledgement. This research was supported by the DFG by grant NE 1564/1-1 (SPP 1158), the European Commission through grant 211384 (EU FP7 “EPOCA”), and the German Federal Ministry of Education and Research (BMBF, FKZ 03F0608, “BIOACID”).

References

Behrends, G., Kuhn, L. T., Ubic, R., and Heuer, A. H.: Raman spectra of vaterite calcium carbonate, Spectrosc. Lett., 28, 983–995, 1995.

Bischoff, W. D., Sharma, S. K., and Mackenzie, F. T.: Carbonate ion disorder in synthetic and biogenic magnesian calcites: a Raman spectral study, Amer. Mineral., 70, 581–589, 1985.

Bøggild, B.: The shell structure of the molluscs, D. Kgl. Danske Vidensk. Selsk. Skr., Naturvidensk. Mathem. 9, 231–326, 1930.

BGD

8, 5563–5585, 2011

Crenshaw, M. A.: The soluble matrix from Mercenaria mercenaria shell, Biomineralization, 6, 6–11, 1972.
Cuif, J.-P., Dauphin, Y., and Sorauf, J. E.: Biominerals and Fossils Through Time, Cambridge University Press, Cambridge, 2011.
Cusack, M., Dauphin, Y., Cuif, J.-P., Salomé, M., Freer, A., and Yin, H.: Micro-XANES mapping of sulphur and its association with magnesium and phosphorus in the shell of the brachiopod, *Terebratulina retusa*, Chem. Geol., 253, 172–179, 2008.
Dauphin, Y. and Denis, A.: Structure and composition of the aragonitic crossed lamellar layers in six species of Bivalvia and Gastropoda, Comp. Biochem. Physiol. A, 126, 367–377, 2000.
Dauphin, Y., Ball, A. D., Cotte, M., Cuif, J.-P., Meibom, A., Salome, M., Susini, J., and Williams, C. T.: Structure and composition of the nacre-prisms transition in the shell of *Pinctada margaritifera* (Mollusca, Bivalvia), Anal. Bioanal. Chem., 390, 1659–1669, 2008.
Dauphin, Y., Brunelle, A., Cotte, M., Cuif, J., Farre, B., Laprévote, O., Meibom, A., Salomé, M., and Williams, C.: A layered structure in the organic envelopes of the prismatic layer of the shell of the pearl oyster *Pinctada margaritifera* (Mollusca, Bivalvia), Microsc. Microanal., 16, 91–98, 2010.
Farre, B. and Dauphin, Y.: Lipids from the nacreous and prismatic layers of two Pteriomorpha Mollusc shells, Comp. Biochem. Physiol. B, 152, 103–109, 2009.
Farre, B., Brunelle, A., Laprévote, O., Cuif, J. P., Williams, C. T., and Dauphin, Y.: Shell layers of the black-lip pearl oyster *Pinctada margaritifera*: matching microstructure and composition, Comp. Biochem. Physiol. B, 159, 131–139, 2011.
Fritsch, E. and Karampelas, S.: Comment on "Determination of carotenoid as the purple pigment in *Gorgonia ventalina* sclerites using Raman spectroscopy" [Leverette et al., Spectrochim. Acta A, 69, 1058–1061, 2008], Spectrochim. Acta, 71(4), 1627, 2008.
Gregoire, C.: Further studies on structure of the organic components in mother-of-pearl, especially in Pelecypods, Bull. Inst. Roy. Sci. Nat. Belg., 36(23), 1–22, 1960.
Hedegaard, D., C., Bardeau, C., and Chateigner, J. F.: Molluscan shell pigments : an in situ resonance raman study, J. Molluscan Stud., 72, 157–162, 2005.
Heim, C., Sjövall, P., Lausmaa, J., Leefmann, T., and Thiel, V.: Spectral characterisation of eight glycerolipids and their detection in natural samples using time-of-flight secondary ion mass spectrometry, Rapid Commun. Mass Spectrom., 23, 2741–2753, 2009.
Karampelas, S.: Etude du changement de couleur des perles par traitement, Ph.D., Université de Nantes, 2008.

BGD
8, 5563–5585, 2011

Kobayashi, I.: Introduction to the shell structure of bivalvian molluscs, Earth Sci., 73, 1–12, 1964.
Kobayashi, I. and Akai, J.: Twinned aragonite crystals found in the bivalvian crossed lamellar shell structure, J. Geol. Soc. Japan, 100, 177–179, 1994.
Krampitz, G., Engels, J., and Cazaux, C.: Biochemical studies on water-soluble proteins and related components of gastropod shells, in: The Mechanisms of Mineralization in the Invertebrates and Plants, edited by: Watabe, N. and Wilbur, K. M., The Belle Baruch Library in Marine Science, Univ. of South Carolina Press, 155–173, 1976.
Kranz, S. A., Wolf-Gladrow, D., Nehrke, G., Langer, G., and Rost, B.: Calcium carbonate precipitation induced by the growth of the marine cyanobacteria *Trichodesmium*, Limnol. Oceanogr., 55, 2563–2569, 2010.
McCrea, J. M.: On the isotopic chemistry of carbonates and a paleotemperature scale, J. Chem. Phys., 18, 849–857, 1950.
Merlin, J. C.: Resonance Raman spectroscopy of carotenoids and carotenoid-containing systems, Pure Appl. Chem., 57(5), 785–792, 1985.
Mutvei, H.: On the micro- and ultrastructure of the conchiolin in the nacreous layer of some recent and fossil molluscs, Stockholm Contr. Geol., 20, 1–17, 1969.
Nakahara, H. and Bevelander, G.: The formation and growth of the prismatic layer of *Pinctada radiata*, Calc. Tiss. Res., 7, 31–45, 1971.
Nudelman, F., Gotliv, B. A., Addadi, L., and Weiner, S.: Mollusk shell formation: mapping the distribution of organic matrix components underlying a single aragonitic tablet in nacre, J. Struct. Biol., 153, 176–187, 2006.
Royal Society: Ocean acidification due to increasing atmospheric carbon dioxide, London: The Royal Society, p. 60, 2005.
Samata, T., Sanguansri, P., Cazaux, C., Hamm, M., Engels, J., and Krampitz, G.: Biochemical studies on components of molluscs shells. The mechanisms of biomineralization in animals and plants, in: Proc. Third Intern. Biomin. Symp., edited by: Omori, M. and Watabe, N., Tokai Univ. Press, Tokai, 37–47, 1980.
Smith, E., Dent, G., and Smith, A.: Modern Raman Spectroscopy: a Practical Approach, John Wiley & Sons, New York, 2005.
Taylor, J. D., Kennedy, W. J., and Hall, A.: The shell structure and mineralogy of the Bivalvia. I. Introduction. Nuculacae – Trigonacae, Bull. Br. Mus. Nat. Hist. Zool., 3, 1–125, 1969.
Travis, D. F.: The structure and organization of, and the relationships between, the inorganic

BGD
8, 5563–5585, 2011

crystals and the organic matrix of the prismatic region of *Mytilus edulis*, J. Ultrastruct. Res., 23, 183–215, 1968.

Urey, H., Lowenstam, H., Eppstein, H., and McKinney, C.: Measurement of paleotemperatures and temperatures of the upper cretaceous of England, Denmark, and the Southeastern United States, Geol. Soc. Amer. Bull., 62, 399–416, 1951.

Urmos, J., Sharma, S. K., and Mackenzie, F. T.: Characterization of some biogenic carbonates with Raman spectroscopy, Amer. Mineral., 76, 641–646, 1991.

Weiner, S. and Traub, W.: Macromolecules in mollusc shells and their functions in biomineralizationk, Philos. Trans. R. Soc. Lond. B, 304, 425–434, 1984.

Wilmot, N. V., Barber, D. J., Taylor, J. D., and Graham, A. L.: Electron microscopy of molluscan crossed-lamellar microstructure, Phil. Trans. R. Soc. Lond. B, 337, 21–35, 1992.

BGD

8, 5563–5585, 2011

Table 1. Experimental parameters of the different mappings performed by means of confocal Raman microscopy.

Label	Scan type	Size (µm)	Points per line	Objective	Wavelength (nm)	Integration time (s)
Scan1a	High resolution	170 × 170	450 × 450	100 × 0.9	785	0.2
Scan1b	Depth profile	100 × 20	200 × 40	100 × 0.9	785	0.1
Scan2a	High resolution	175 × 175	450 × 450	100 × 0.9	532	0.2
Scan2b	Large area	1500 × 700	450 × 450	20 × 0.4	532	0.1
Scan1c	High resolution	175 × 175	450 × 450	100 × 0.9	532	0.2

BGD
8, 5563–5585, 2011

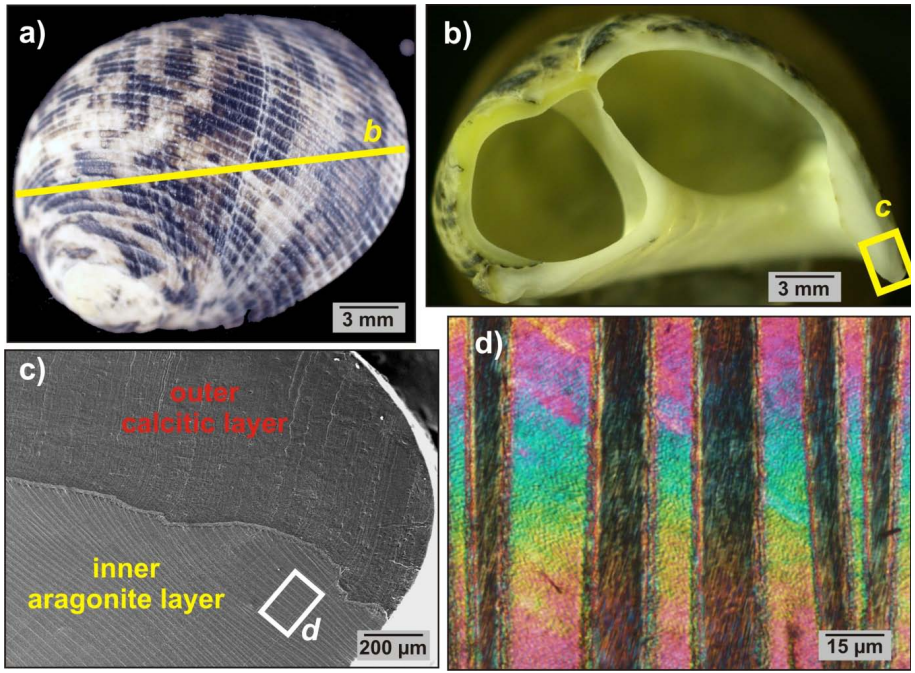

Fig. 1. (a) Picture showing the shell of *Nerita undata*. Line indicates where the specimen was cut. **(b)** Cross section of the shell along radial axis. **(c)** SEM micrograph of a section across the outer lip close to the aperture of the shell. **(d)** Thin section of the aragonitic cross lamellar structure forming the inner layer of the shell observed using polarized light microscopy (with crossed polars).

BGD
8, 5563–5585, 2011

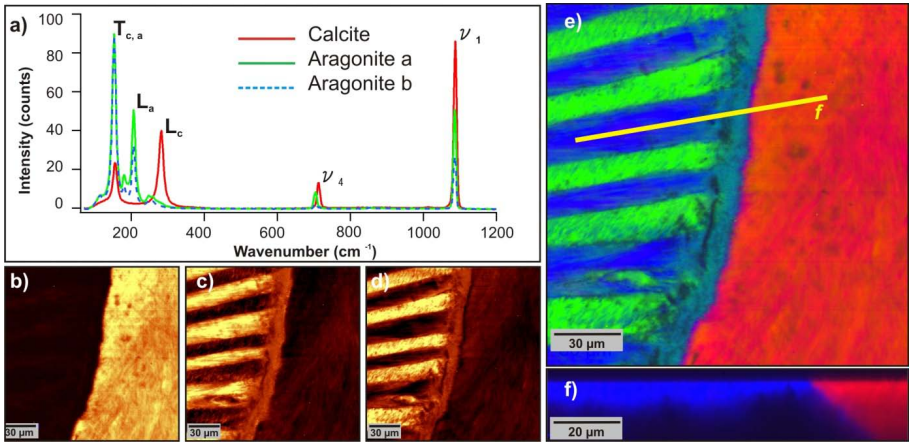

Fig. 2. **(a)** Raman spectra of calcite and aragonite extracted from scan1a (aragonite_a and aragonite_b are related to different crystallographic orientations). **(b)** Map showing the distribution of calcite across the area scanned in scan1a. **(c)** Map showing the distribution of aragonite_a across the area scant in scan1a. **(d)** Map showing the distribution of aragonite_b across the area scanned in scan1a. **(e)** False color composite of maps **(b–d)**. Line f marks the transect along which a depth scan (scan1b) was performed. **(f)** False color composite showing the vertical distribution of calcite and aragonite along transect f **(e)** determined from scan1b.

BGD
8, 5563–5585, 2011

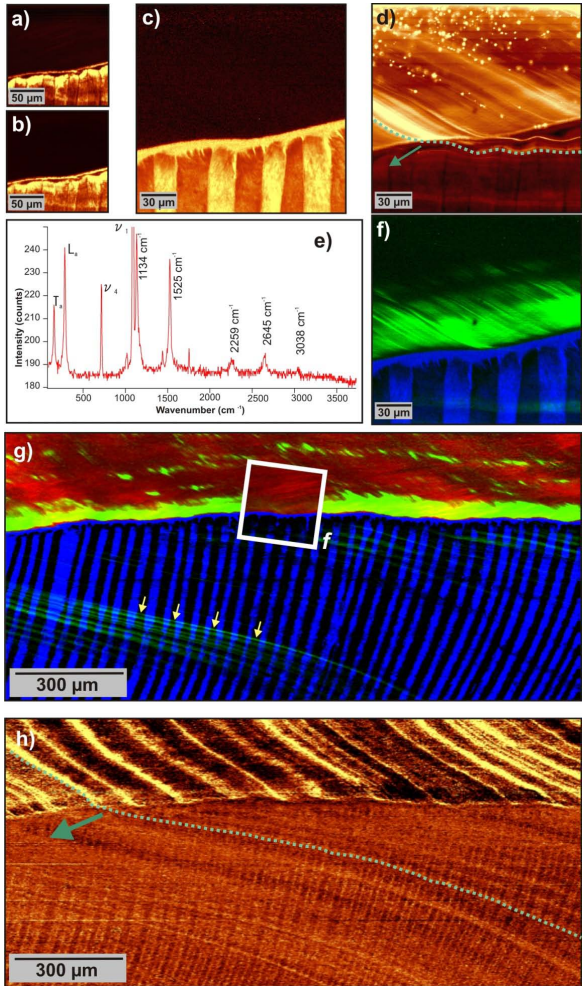

Fig. 3. (Caption on next page.)

BGD
8, 5563–5585, 2011

Fig. 3. **(a)** Map showing the intensity distribution (peak area) of the lattice peak of aragonite (translation mode T_a at 152 cm^{-1}) extracted from scan2a. **(b)** Map showing the intensity distribution of the lattice peak (peak area) of aragonite (liberation mode L_a, 206 cm^{-1}). **(c)** Map calculated from the ratio of map (**a** and **b**). **(d)** Map showing the intensity distribution of the background intensity (between 2400 cm^{-1} and 2500 cm^{-1}) related to the fluorescence of the sample. **(e)** Raman spectra extracted from scan2a showing the typical aragonite spectra and the RR peaks related to the presence of polyenes. **(f)** Map calculated from scan2a showing the distribution of the polyenes (green). **(g)** Map showing the distribution of calcite (red), aragonite_a (black), aragonite_b (blue), and polyenes (green) as extracted from scan2b. The area f indicates the area in which the previous scan (scan2a) was performed. The arrows in the aragonitic domain highlight where polyenes visualize the growth lines of the shell. **(h)** Map showing the change in full width half maximum (FWHM) of the symmetric stretch ν_1 of carbonate group at 1085 cm^{-1} extracted from scan2b.

BGD
8, 5563–5585, 2011

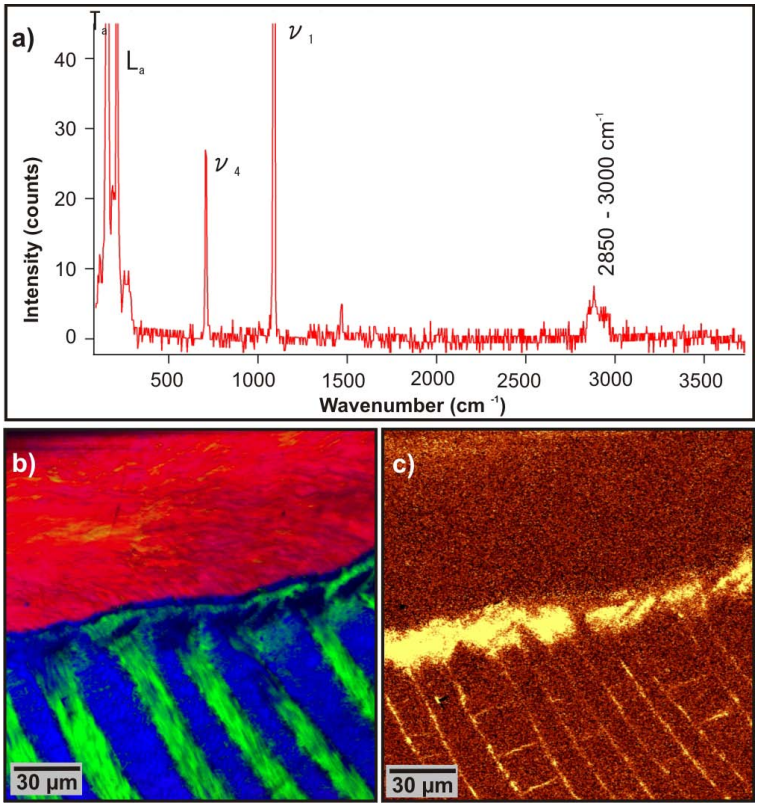

Fig. 4. **(a)** Raman spectra extracted from scan1c showing the typical aragonite spectra and peaks between 2850–3000 cm^{-1} which correspond to the spectral range for –C–H groups stretching vibrations. **(b)** Map showing the intensity distribution of calcite (red), aragonite_a (green), and aragonite_b (blue) extracted from scan1c. **(c)** Map showing the intensity distribution of the peak between 2850–3000 cm^{-1} which correspond to the spectral range for –C–H groups stretching vibrations as extracted from scan1c.

BGD
8, 5563–5585, 2011